Complex-valued eikonal-transport equation

Luděk Klimeš

Department of Geophysics, Faculty of Mathematics and Physics, Charles University, Ke Karlovu 3, 121 16 Praha 2, Czech Republic, http://sw3d.cz/staff/klimes.htm

Summary

It is well known that the representation of amplitude variations in terms of complex–valued travel time increases the accuracy of the ray methods. In order to represent the amplitude variations in terms of complex–valued travel time, we supplement the eikonal equation for complex–valued travel time with the frequency–dependent term corresponding to the transport equation. We refer to this equation for the complex–valued travel time including amplitude variations as the "eikonal–transport equation".

In real space, the eikonal–transport equation for complex–valued travel time represents the system of two second–order partial differential equations for the real and imaginary parts of the complex–valued travel time. The solution of this system of equations does not propagate along rays, and has to be solved by suitable numerical methods.

We propose to consider a system of surfaces and to calculate the complex–valued travel time from one surface to the subsequent surface numerically, analogously to the system of two Hamilton–Jacobi equations for complex–valued travel time. This method may be suitable for application to wavefront tracing.

We present two simple numerical examples, including comparisons with the standard ray theory and with the Gaussian beam summation.

Keywords

Wave propagation, complex–valued travel time, amplitude, caustic, eikonal equation, transport equation.

In: Seismic Waves in Complex 3–D Structures, Report 19 (Department of Geophysics, Charles University, Prague, 2009), pp. 173–190

1. Introduction

It is well known that the representation of amplitude variations in terms of complex–valued travel time increases the accuracy of the ray methods. For example, if we represent the initial envelope of a Gaussian beam by the imaginary part of travel time, we usually obtain a reasonable solution. If we represent the initial envelope of a Gaussian beam by amplitude, the evolution of the envelope resulting from the transport equation is incorrect (Kravtsov, personal communication). Unfortunately, even if we represent the initial conditions for amplitude variations in terms of complex–valued travel time and put the initial amplitude constant, the solution of the transport equation for amplitude may gradually produce severe amplitude variations.

In order to represent the amplitude variations in terms of complex–valued travel time everywhere, we supplement the eikonal equation for complex–valued travel time with the frequency–dependent term corresponding to the transport equation. We refer to this equation for the complex–valued travel time including amplitude variations as the *eikonal–transport equation.*

In real space, the eikonal–transport equation for complex–valued travel time represents the system of two second–order partial differential equations for the real and imaginary parts of the complex–valued travel time. The solution of this system of equations does not propagate along rays, and has to be solved by suitable numerical methods. For high frequencies, the complex–valued solution of the eikonal–transport equation approaches the solution of the system of Hamilton–Jacobi equations for complex–valued travel time.

Unfortunately, the eikonal–transport equation suffers from various problems, which have to be solved before the eikonal–transport equation can become applicable. Refer to Section 2.4 for examples of these problems.

In this paper, we propose to consider a system of surfaces and to calculate the complex–valued travel time from one surface to the subsequent surface numerically, analogously to the system of two Hamilton–Jacobi equations for complex–valued travel time (Klimeš, 2009). This method may be suitable for application to wavefront tracing (Vinje, Iversen & Gjøystdal, 1993; Vinje et al., 1996). It is obvious that this numerical solution of the eikonal–transport equation for complex–valued travel time will suffer from all numerical problems relevant to the numerical solution of the system of two Hamilton–Jacobi equations.

We introduce the eikonal–transport equation in Section 2. We then propose one alternative for numerically solving the eikonal–transport equation in Section 3. Another alternative, not yet studied, consists in application of finite differences in all spatial directions. We present two simple numerical examples, including comparisons with the standard ray theory and with the Gaussian beam summation, in Sections 4 and 5.

Lower–case roman indices $a, b, ... = 1, 2, 3$ correspond to spatial coordinates, and upper–case roman indices $A, B, ... = 1, 2$ correspond to two spatial directions along the chosen surfaces. Lower–case greek subscripts index the points along the chosen surfaces. The Einstein summation over repetitive indices is used throughout the paper.

2. Scalar wave equation and the complex–valued eikonal–transport equation

In this paper, we consider scalar wave equation

$$(\varrho v^2 u_{,j})_{,j} + \omega^2 \varrho\, u = 0 \tag{1}$$

for scalar wavefield $u = u(x^k)$ in the frequency domain.

2.1. Amplitude and travel time

We express complex–valued wavefield u in terms of amplitude A and travel time τ,

$$u = A \exp(\mathrm{i}\omega\tau) \quad . \tag{2}$$

We insert (2) into wave equation (1) and obtain

$$[\varrho v^2 (A_{,j} + \mathrm{i}\omega A \tau_{,j}) \exp(\mathrm{i}\omega\tau)]_{,j} + \omega^2 \varrho\, A \exp(\mathrm{i}\omega\tau) = 0 \quad . \tag{3}$$

We differentiate the product in the first term and arrive at

$$\varrho v^2 (A_{,j} + \mathrm{i}\omega A\tau_{,j})\mathrm{i}\omega\tau_{,j} + [\varrho v^2 (A_{,j} + \mathrm{i}\omega A \tau_{,j})]_{,j} + \omega^2 \varrho\, A = 0 \quad . \tag{4}$$

We sort the terms in (4) according to the powers of $\mathrm{i}\omega$ and obtain scalar wave equation

$$(\mathrm{i}\omega)^2 \varrho\, A\, (v^2 \tau_{,j}\tau_{,j} - 1) + 2\mathrm{i}\omega \sqrt{\varrho}v\, (\sqrt{\varrho}vA)_{,j}\tau_{,j} + \mathrm{i}\omega \varrho v^2 A\, \tau_{,jj} + (\varrho v^2 A_{,j})_{,j} = 0 \; . \tag{5}$$

2.2. Standard ray series

Equation (5) is usually solved in terms of the standard ray series

$$A = \sum_{n=0}^{+\infty} (\mathrm{i}\omega)^{-n} A^{[n]} \quad . \tag{6}$$

We insert ray series (6) into equation (5), collect the terms corresponding to equal powers of $\mathrm{i}\omega$, and put the sums equal to zero.

For $(\mathrm{i}\omega)^2$, we obtain eikonal equation for travel time

$$v^2\, \tau_{,j}\tau_{,j} - 1 = 0 \quad . \tag{7}$$

For $(\mathrm{i}\omega)^1$, we obtain transport equation for $A^{[0]}$

$$(\sqrt{\varrho}vA^{[0]})_{,j}\tau_{,j} + \tfrac{1}{2}\sqrt{\varrho}vA^{[0]}\tau_{,jj} = 0 \quad . \tag{8}$$

For $(\mathrm{i}\omega)^{1-n}$, we obtain higher–order transport equations for $A^{[n]}$, $n > 0$,

$$(\sqrt{\varrho}vA^{[n]})_{,j}\tau_{,j} + \tfrac{1}{2}\sqrt{\varrho}vA^{[n]}\tau_{,jj} + \tfrac{1}{2}(\sqrt{\varrho}v)^{-1}(\varrho v^2 A^{[n-1]}_{,j})_{,j} = 0 \quad . \tag{9}$$

Approximate solution of the wave equation obtained by restricting ray series (6) to terms corresponding to $n = 0, 1, ..., N$ is usually referred to as the N^{th}–order ray–theory approximation. The wavefield error of the N^{th}–order ray–theory approximation is of order $O(\omega^{-N-1})$.

2.3. Complex–valued travel time in place of amplitude

We try to incorporate the amplitude into the imaginary part of complex–valued travel time. We choose

$$A = (\sqrt{\varrho}v)^{-1} \quad , \tag{10}$$

insert (10) into (5), and obtain equation

$$\tau_{,j}\tau_{,j} - v^{-2} + (\mathrm{i}\omega)^{-1}\tau_{,jj} - (\mathrm{i}\omega)^{-2}(\sqrt{\varrho}v)^{-1}(\sqrt{\varrho}v)_{,jj} = 0 \tag{11}$$

for frequency–dependent complex–valued travel time. We shall refer to equation (11) as the *eikonal–transport equation*. We define

$$w = \tfrac{1}{2}[v^{-2} - \omega^{-2}(v\sqrt{\varrho})^{-1}(v\sqrt{\varrho})_{,jj}] \quad , \tag{12}$$

and express eikonal–transport equation (11) in simple form

$$\boxed{\tau_{,j}\tau_{,j} = 2w + \tfrac{\mathrm{i}}{\omega}\,\tau_{,jj} \quad . \qquad (13)}$$

Note that the difference between frequency–dependent w and $\frac{1}{2}v^{-2}$ is negligible in velocity models suitable for application of ray methods.

Complex–valued eikonal–transport equation (13) is formally equivalent to scalar wave equation (1), but considerable differences may arise from boundary conditions.

2.4. Problems in the eikonal–transport equation

The representation of the amplitude by the complex–valued travel time may induce various problems.

For example, at zero isosurfaces of the wavefield amplitude (nodal surfaces), the imaginary part of travel time has a logarithmic singularity and the real part of travel time has a discontinuity of π/ω. This prevents a numerical solution of the eikonal–transport equation in vicinities of nodal surfaces.

If we represent the interference of two or more waves by a single–valued travel time, the solution of the eikonal–transport equation oscillates and the proposed method becomes inefficient and numerically unstable. This typically happens beyond caustics. Let us consider the interference

$$u = (1-a)\,\exp(\mathrm{i}\omega\tau^1) + a\,\exp(\mathrm{i}\omega\tau^2) \tag{14}$$

of two waves. For very small a,

$$u = \exp(\mathrm{i}\omega\tau^1)\left\{1 - a + a\,\exp[\mathrm{i}\omega(\tau^2-\tau^1)]\right\} \quad , \tag{15}$$

and complex–valued travel time

$$\tau = \tfrac{1}{\mathrm{i}\omega}\,\ln(u) \tag{16}$$

approximately reads

$$\tau \approx \tau^1 + \tfrac{a}{\mathrm{i}\omega}\left\{\exp[\mathrm{i}\omega(\tau^2-\tau^1)] - 1\right\} \quad . \tag{17}$$

This equation represents travel–time oscillations with amplitude a/ω and local wavelength $2\pi/(\omega|\tau^2_{,i}-\tau^1_{,i}|)$. For $a = \frac{1}{2}$,

$$u = \exp(\mathrm{i}\omega\tfrac{\tau^1+\tau^2}{2})\,\cos(\omega\tfrac{\tau^2-\tau^1}{2}) \quad , \tag{18}$$

complex–valued travel time (16) reads

$$\tau = \tfrac{\tau^1+\tau^2}{2} + \tfrac{1}{\mathrm{i}\omega}\,\ln[\cos(\omega\tfrac{\tau^2-\tau^1}{2})] \quad , \tag{19}$$

and we encounter logarithmic singularities repeating with interval $2\pi/(\omega|\tau^2_{,i}-\tau^1_{,i}|)$.

3. Numerical high–frequency asymptotic solution of the complex–valued eikonal–transport equation

We shall try to solve the complex–valued eikonal–transport equation by a method similar to wavefront tracing, analogously to the complex–valued eikonal equation (Klimeš, 2009). We shall consider a system of surfaces and calculate the complex–valued travel time from one surface to the subsequent surface.

The applicability and accuracy of this method will obviously depend on the selection of these surfaces in the first place. In the second place, the applicability and accuracy of the method will depend on the selection of discrete points at the surfaces for sampling the complex–valued travel time. Note that the system of surfaces for calculating the complex–valued travel time should respect the multi–valued nature of travel time, which implies that the selection of the surfaces will constitute a very difficult task.

We assume that the values $\tau(x^m_\alpha)$ of the complex–valued travel time are known at given discrete points x^m_α situated at a given surface. For more accurate methods, we assume to know also the values of the derivatives of complex–valued travel time along the surface. We then calculate these values at corresponding points $\widetilde{x}^m_\alpha$ situated at a close subsequent surface.

At each point x^m_α, we define vector

$$t^i_3 = (\widetilde{x}^i_\alpha - x^i_\alpha)/h_3 \tag{20}$$

leading from point x^m_α at the given surface to corresponding point $\widetilde{x}^m_\alpha$ at the subsequent surface. Here h_3 is the optional step in the independent parameter γ_3 parametrizing the system of surfaces. We may set

$$h_3 = 1 \quad . \tag{21}$$

At each point x^m_α, we denote two vectors tangent to the given surface by t^i_1 and t^i_2. Vectors t^i_1 and t^i_2 can be determined from the positions of several given points situated close to point x^m_α at the given surface so as to optimize the finite–difference scheme for numerical determination of derivatives in the directions of these vectors. We shall refer to the derivatives in the directions of vectors t^i_1 and t^i_2 as the *lateral derivatives*.

We introduce covariant vectors $\hat{t}^1_i$, $\hat{t}^2_i$ and $\hat{t}^3_i$ biorthonormal to t^i_1, t^i_2 and t^i_3,

$$\hat{t}^a_i \, t^k_a = \delta^k_i \quad . \tag{22}$$

Then

$$G^{ab} = \hat{t}^a_i \, \hat{t}^b_i \tag{23}$$

is the contravariant metric tensor corresponding to local basis vectors t^i_1, t^i_2 and t^i_3.

We define the derivatives of complex–valued travel time covariantly transformed to vectors t^j_a,

$$T_a = \tau_{,i} \, t^i_a \quad , \tag{24}$$

$$T_{ab} = \tau_{,ij} \, t^i_a \, t^j_b \quad , \tag{25}$$

$$T_{abc} = \tau_{,ijk} \, t^i_a \, t^j_b \, t^k_c \quad , \tag{26}$$

$$T_{abcd} = \tau_{,ijkl} \, t^i_a \, t^j_b \, t^k_c \, t^l_d \quad , \tag{27}$$

$$T_{abcde} = \tau_{,ijklm} \, t^i_a \, t^j_b \, t^k_c \, t^l_d \, t^m_e \quad , \tag{28}$$

and so on.

We also define the derivatives of (12) covariantly transformed to vectors t_a^j,

$$W_a = w_{,i}\, t_a^i \quad , \tag{29}$$

$$W_{ab} = w_{,ij}\, t_a^i\, t_b^j \quad , \tag{30}$$

$$W_{abc} = w_{,ijk}\, t_a^i\, t_b^j\, t_c^k \quad , \tag{31}$$

and so on.

We differentiate complex–valued eikonal–transport equation (13) with respect to x^j,

$$\tau_{,i}\tau_{,ij} = w_{,j} + \tfrac{\mathrm{i}}{2\omega}\, \tau_{,iij} \quad . \tag{32}$$

We differentiate equation (32) with respect to x^k,

$$\tau_{,i}\tau_{,ijk} = w_{,jk} - \tau_{,ij}\tau_{,ik} + \tfrac{\mathrm{i}}{2\omega}\, \tau_{,iijk} \quad . \tag{33}$$

We differentiate equation (33) with respect to x^l,

$$\tau_{,i}\tau_{,ijkl} = w_{,jkl} - \tau_{,ij}\tau_{,ikl} - \tau_{,ik}\tau_{,ijl} - \tau_{,il}\tau_{,ijk} + \tfrac{\mathrm{i}}{2\omega}\, \tau_{,iijkl} \quad , \tag{34}$$

and so on.

We transform equations (13) and (32)–(34) to vectors t_a^j. Equation (13) then reads

$$T_g G^{gh} T_h = 2w + \tfrac{\mathrm{i}}{\omega}\, G^{gh} T_{gh} \quad . \tag{35}$$

Equation (32) reads

$$T_g G^{gh} T_{ha} = W_a + \tfrac{\mathrm{i}}{2\omega}\, G^{gh} T_{gha} \quad . \tag{36}$$

Equation (33) reads

$$T_g G^{gh} T_{hab} = W_{ab} - T_{ag} G^{gh} T_{hb} + \tfrac{\mathrm{i}}{2\omega}\, G^{gh} T_{ghab} \quad . \tag{37}$$

Equation (34) reads

$$T_g G^{gh} T_{habc} = W_{abc} - T_{ag} G^{gh} T_{hbc} - T_{bg} G^{gh} T_{hac} - T_{cg} G^{gh} T_{hab} + \tfrac{\mathrm{i}}{2\omega}\, G^{gh} T_{ghabc} \; , \tag{38}$$

and so on.

We now rearrange equations (36), (37) and (38),

$$T_{3a} = (T_g G^{g3})^{-1} (W_a - T_g G^{gH} T_{Ha} + \tfrac{\mathrm{i}}{2\omega}\, G^{gh} T_{gha}) \quad , \tag{39}$$

$$T_{3ab} = (T_g G^{g3})^{-1} (W_{ab} - T_{ag} G^{gh} T_{hb} - T_g G^{gH} T_{Hab} + \tfrac{\mathrm{i}}{2\omega}\, G^{gh} T_{ghab}) \quad . \tag{40}$$

$$\begin{aligned} T_{3abc} = (T_g G^{g3})^{-1} (W_{abc} &- T_{ag} G^{gh} T_{hbc} - T_{bg} G^{gh} T_{hac} - T_{cg} G^{gh} T_{hab} \\ &- T_g G^{gH} T_{Habc} + \tfrac{\mathrm{i}}{2\omega}\, G^{gh} T_{ghabc}) \quad , \end{aligned} \tag{41}$$

and so on.

For given T_A, equation (35) represents the quadratic equation for T_3. Its solution reads

$$T_3 = \sqrt{(G^{33})^{-1} \left[2w - T_G G^{GH} T_H + (G^{33})^{-1} (G^{3H} T_H)^2 + \tfrac{\mathrm{i}}{\omega}\, G^{gh} \underline{T_{gh}} \right]} - (G^{33})^{-1} G^{3H} T_H \; . \tag{42}$$

Equations (39)–(41) read

$$T_{A3} = (T_g G^{g3})^{-1} (W_A - T_g G^{gH} T_{HA} + \tfrac{\mathrm{i}}{2\omega}\, G^{gh} \underline{T_{ghA}}) \quad , \tag{43}$$

$$T_{33} = (T_g G^{g3})^{-1} (W_3 - T_g G^{gH} T_{H3} + \tfrac{\mathrm{i}}{2\omega}\, G^{gh} \underline{T_{gh3}}) \quad , \tag{44}$$

$$T_{AB3} = (T_g G^{g3})^{-1} (W_{AB} - T_{Ag} G^{gh} T_{hB} - T_g G^{gH} T_{HAB} + \tfrac{\mathrm{i}}{2\omega} G^{gh} \underline{T_{ghAB}}) \quad , \tag{45}$$

$$T_{A33} = (T_g G^{g3})^{-1} (W_{A3} - T_{Ag} G^{gh} T_{h3} - T_g G^{gH} T_{HA3} + \tfrac{\mathrm{i}}{2\omega} G^{gh} \underline{T_{ghA3}}) \quad , \tag{46}$$

$$T_{333} = (T_g G^{g3})^{-1} (W_{33} - T_{3g} G^{gh} T_{h3} - T_g G^{gH} T_{H33} + \tfrac{\mathrm{i}}{2\omega} G^{gh} \underline{T_{gh33}}) \quad , \tag{47}$$

$$\begin{aligned} T_{ABC3} = (T_g G^{g3})^{-1} (W_{ABC} &- T_{Ag} G^{gh} T_{hBC} - T_{Bg} G^{gh} T_{hAC} - T_{Cg} G^{gh} T_{hAB} \\ &- T_g G^{gH} T_{HABC} + \tfrac{\mathrm{i}}{2\omega} G^{gh} \underline{T_{ghABC}}) \quad , \end{aligned} \tag{48}$$

$$\begin{aligned} T_{AB33} = (T_g G^{g3})^{-1} (W_{AB3} &- T_{Ag} G^{gh} T_{hB3} - T_{Bg} G^{gh} T_{hA3} - T_{3g} G^{gh} T_{hAB} \\ &- T_g G^{gH} T_{HAB3} + \tfrac{\mathrm{i}}{2\omega} G^{gh} \underline{T_{ghAB3}}) \quad , \end{aligned} \tag{49}$$

$$\begin{aligned} T_{A333} = (T_g G^{g3})^{-1} (W_{A33} &- T_{Ag} G^{gh} T_{h33} - 2 T_{3g} G^{gh} T_{hA3} \\ &- T_g G^{gH} T_{HA33} + \tfrac{\mathrm{i}}{2\omega} G^{gh} \underline{T_{ghA33}}) \quad , \end{aligned} \tag{50}$$

$$\begin{aligned} T_{3333} = (T_g G^{g3})^{-1} (W_{333} &- 3 T_{3g} G^{gh} T_{h33} \\ &- T_g G^{gH} T_{H333} + \tfrac{\mathrm{i}}{2\omega} G^{gh} \underline{T_{gh333}}) \quad , \end{aligned} \tag{51}$$

and so on.

We may calculate the complex–valued travel time and possibly its some lower–order lateral derivatives by a suitable method of numerical integration, e.g., by Runge–Kutta. We than calculate the remaining required lateral derivatives T_{AB}, T_{ABC}, T_{ABCD}, ... by finite differences. Other derivatives are then determined by equations (42)–(51) and analogous higher–order equations.

Analogously to the ray–theory approximation, we refer to an approximate solution of the eikonal–transport equation as the N^{th}–order eikonal–transport approximation if the high–frequency asymptotic order of the corresponding wavefield error is $O(\omega^{-N-1})$.

Equation (42) with $T_{ab} = 0$ represents the eikonal equation only. Equations (42)–(44) with $T_{abc} = 0$ represent a zero–order eikonal–transport approximation. Equations (42)–(47) with $T_{abcd} = 0$ represent a first–order eikonal–transport approximation. Equations (42)–(51) with $T_{abcde} = 0$ represent a second–order eikonal–transport approximation. In general, if we put the $(N+3)^{\mathrm{rd}}$–order and higher–order travel–time derivatives equal to zero, the above equations represent the N^{th}–order eikonal–transport approximation. Note that we may neglect also some other higher–order terms and still maintain the order of eikonal–transport approximation.

We may calculate the travel–time derivatives up to the M^{th}–order by a suitable method of numerical integration, e.g., Runge–Kutta. In this case, we have to consider the derivatives of the calculated derivatives up to the $(N+2)^{\mathrm{nd}}$–order in order to obtain the N^{th}–order eikonal–transport approximation. For example, if we calculate complex–valued travel time and it first–order derivatives by Runge–Kutta and wish to obtain the first–order eikonal–transport approximation, we need the third–order derivatives of the calculated first–order derivatives, i.e., we need to calculate the first–order to fourth–order travel–time derivatives using equations (42)–(51) with $T_{abcde} = 0$.

Equations (42)–(51) can be solved iteratively. We put the initial values of the underlined derivatives $\underline{T_{...}}$ equal to zero, and iteratively execute equations (42)–(44), then (42)–(47), then (42)–(51), and so on. We then execute several times all selected equations, until we reach the specified number of iterations.

We propose here to calculate lateral derivatives $T_A(x^m_\alpha)$ by numerical integration of equation (43). Travel time $\tau(x^m_\alpha)$ is obtained by numerical quadrature of equation (42). The lateral derivatives of travel time $\tau(x^m_\alpha)$ then slowly but steadily become different from $T_A(x^m_\alpha)$. In order to maintain a relation between $T_A(x^m_\alpha)$ and the lateral derivatives of $\tau(x^m_\alpha)$, we may apply modification

$$T_A(x^m_\alpha) \longrightarrow T_A(x^m_\alpha) + q\left[T^{\mathrm{FD}}_A(x^m_\alpha) - T_A(x^m_\alpha)\right] \tag{52}$$

with small coefficient q during each step of numerical integration. Here $T^{\mathrm{FD}}_A(x^m_\alpha)$ are calculated from $\tau(x^m_\alpha)$ by finite differences.

4. Numerical example for a constant vertical velocity gradient

In the 1–D model with constant vertical velocity gradient, the velocity increases linearly with depth, and the density is constant. The 2–D model volume is represented by a vertical square. The ratio of the real–valued velocity between top and bottom is 1:3, and the velocity gradient is $-2\,\mathrm{s}^{-1}$. If we assume that the dimensions of the square are $1\,\mathrm{km}\times 1\,\mathrm{km}$, the velocity is $1\,\mathrm{km\,s^{-1}}$ at the top and $3\,\mathrm{km\,s^{-1}}$ at the bottom. The point source is situated at the left–hand top corner of the square. The model was used by Podvin & Lecomte (1991) to study the accuracy of their first–order grid travel–time tracing method, and also by Klimeš (1996).

In order to make coding the numerical solution of the eikonal–transport equation for complex–valued travel time as simple as possible, we coded very primitive version analogous to the solution of the complex–valued eikonal equation by Klimeš (2009), in which the system of surfaces for calculation of travel time is formed by vertical lines.

Since this primitive version obviously cannot be applied in the vicinity of the point source, we calculate the complex–valued travel time in the right–hand half of the vertical square only. If we introduce horizontal coordinate x^1 extending from $x^1 = 0.000\,\mathrm{km}$ at the left–hand side of the square to $x^1 = 1.000\,\mathrm{km}$ at the right–hand side and vertical coordinate x^3 extending from $x^3 = -1.000\,\mathrm{km}$ at the bottom to $x^3 = 0.000\,\mathrm{km}$ at the top, the point source is located at $x^1 = 0.000\,\mathrm{km}$, $x^3 = 0.000\,\mathrm{km}$, and we calculate the complex–valued travel time from $x^1 = 0.500\,\mathrm{km}$ to $x^1 = 1.000\,\mathrm{km}$. The initial complex–valued travel time and its vertical derivative are calculated analytically along the vertical line situated at $x^1 = 0.500\,\mathrm{km}$. The real part of the initial travel time equals the real–valued travel time from the point source. The imaginary part

$$\mathrm{Im}(\tau) = -\tfrac{1}{\omega}\ln(A) \tag{53}$$

of the initial travel time describes the amplitude A corresponding to the point source. The spacing between subsequent vertical lines for calculation of travel time is $0.005\,\mathrm{km}$. We thus have 101 vertical lines between $x^1 = 0.500\,\mathrm{km}$ and $x^1 = 1.000\,\mathrm{km}$. We select 201 discrete points along each vertical line between $x^3 = -1.000\,\mathrm{km}$ and $x^3 = 0.000\,\mathrm{km}$.

In these coordinates, we choose

$$\begin{pmatrix} t^1_1 & t^1_3 \\ t^3_1 & t^3_3 \end{pmatrix} = \begin{pmatrix} 0 & 1 \\ 1 & 0 \end{pmatrix} \quad . \tag{54}$$

We then calculate two complex values

$$\tau(x^m_\alpha) \quad , \qquad T_1(x^m_\alpha) = \tau_{,3}(x^m_\alpha) \tag{55}$$

at each of 201 points along a vertical line. Along each vertical line, we calculate the lateral derivatives $T^{\mathrm{FD}}_1(x^m_\alpha)$ of $\tau(x^m_\alpha)$, and the lateral derivatives $T_{11}(x^m_\alpha)$ and $T_{111}(x^m_\alpha)$ of

$T_1(x^m_\alpha)$ by simple finite differences from the 3 points nearest to x^m_α (derivative $T_{111}(x^m_\alpha)$ at the endpoints from the 4 nearest points). The derivatives in the horizontal direction are calculated using 3 iterations of equations (42) to (47) with $T_{abcd} = 0$. For stabilization (52), we use $q = 0.002$. We apply fourth–order Runge–Kutta subroutine `RKGS` to the numerical integration of 804 ordinary differential equations in the horizontal direction. We avoid halving the intervals between subsequent vertical lines.

We perform all numerical calculations in single precision. The complex–valued travel time at frequency 200 Hz numerically calculated by the eikonal–transport equation along the 101 vertical lines is displayed in Figures 1 and 2. The maximum differences of the numerical zero–order eikonal–transport solution from the analytical zero–order ray–theory solution at frequency 200 Hz are $1.91{\times}10^{-6}$s for the real part and $0.23{\times}10^{-6}$s for the imaginary part.

The numerical solution of the eikonal–transport equation for complex–valued travel time is very good at high frequencies. At frequency 200 Hz, a localized chequered instability of the lateral first–order derivative of complex–valued travel time is created near the left–hand bottom corner of the computational volume, where the angle between the slowness vector and vector t^i_3 is largest. It is interesting that this local instability rapidly heals, probably because of the reduction of the angle between the slowness vector and vector t^i_3 due to ray bending. This local instability increases when lowering the frequency, becomes global, and destroys the numerical solution before reaching 180 Hz. This instability can be removed by reducing the interval between the surfaces for calculating complex–valued travel time with respect to the interval between discrete points along the surfaces. Unfortunately, reducing the interval between the surfaces increases accumulated numerical errors and the numerical solution becomes inaccurate below 40 Hz.

An exact solution of the eikonal–transport equation (13) yields an exact solution of the scalar wave equation (1), but we applied here the zero–order solution of the eikonal–transport equation according to Section 3. No differences between the analytical zero–order ray–theory solution and the numerical zero–order solution of the eikonal–transport equation other than numerical have been observed above 40 Hz.

5. Numerical example with a caustic in a homogeneous velocity model

In the homogeneous velocity model, the real–valued velocity is $v = 1\,\mathrm{km\,s^{-1}}$, and the density is constant. The 2–D model volume is represented by a vertical square. We assume that the dimensions of the square are $1\,\mathrm{km}\times 1\,\mathrm{km}$. Together with the preceding example, we introduce horizontal coordinate x^1 extending from $x^1 = 0.000$ km at the left–hand side of the square to $x^1 = 1.000$ km at the right–hand side, and vertical coordinate x^3 extending from $x^3 = -1.000$ km at the bottom to $x^3 = 0.000$ km at the top.

The initial complex–valued travel time is given along the left–hand side $x^1 = 0.000$ km of the 2–D model volume. We specify unit initial amplitude, i.e., zero imaginary part of the initial travel time, and the cosine real part of the initial travel time,

$$\tau(x^3) = \frac{1}{v\,x^1_{\mathrm{F}}}\left(\frac{\Lambda}{2\pi}\right)^2 \cos\!\left(\frac{2\pi}{\Lambda}(x^3 - x^3_{\mathrm{F}})\right) \quad . \tag{56}$$

This initial travel time is periodic with interval Λ, and creates a caustic surface, which extends from focal point $x^1 = x^1_{\mathrm{F}}$, $x^3 = x^3_{\mathrm{F}}$ to the right. We choose

$$\Lambda = 0.800\,\mathrm{km} \quad , \qquad x^1_{\mathrm{F}} = 0.700\,\mathrm{km} \quad , \qquad x^3_{\mathrm{F}} = -0.500\,\mathrm{km} \quad . \tag{57}$$

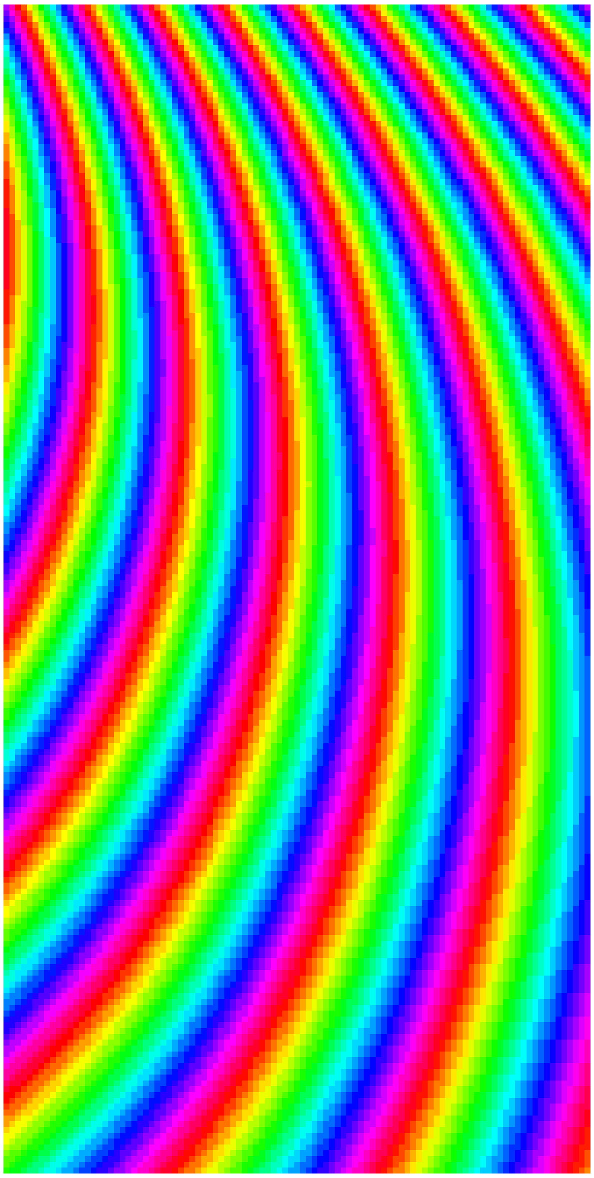

Figure 1. The real part of travel time at frequency 200 Hz, corresponding to the point source located at $x^1 = 0.000\,\mathrm{km}$, $x^3 = 0.000\,\mathrm{km}$ in the real–valued velocity model with velocity $1\,\mathrm{km\,s^{-1}}$ at the top and $3\,\mathrm{km\,s^{-1}}$ at the bottom. The values of the real part of travel time range from 0.441 s to 0.881 s. The colour circle corresponds to the time increment of 0.050 s, i.e., to 10 wavelengths. The yellow colour corresponds to values 0.450 s, 0.500 s, 0.550 s, etc. The maximum difference of the numerical zero–order eikonal–transport solution from the analytical zero–order ray–theory solution is 1.9×10^{-6} s.

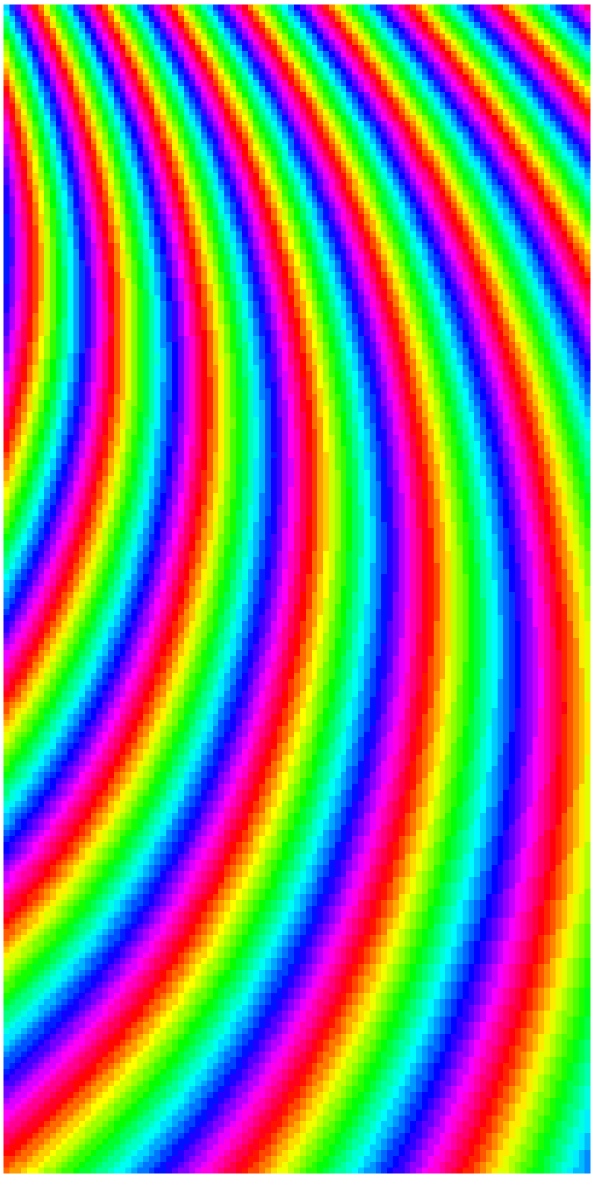

Figure 2. The imaginary part of travel time at frequency 200 Hz, corresponding to the point source located at $x^1 = 0.000\,\mathrm{km}$, $x^3 = 0.000\,\mathrm{km}$ in the real–valued velocity model with velocity $1\,\mathrm{km\,s^{-1}}$ at the top and $3\,\mathrm{km\,s^{-1}}$ at the bottom. The values of the imaginary part of travel time range from -0.276×10^{-3} s to 0.138×10^{-3} s. The colour circle corresponds to the time increment of 0.050×10^{-3} s. The yellow colour corresponds to values -0.250×10^{-3} s, -0.200×10^{-3} s, ..., 0.100×10^{-3} s. The maximum difference of the numerical zero–order eikonal–transport solution from the analytical zero–order ray–theory solution is 0.23×10^{-6} s.

The numerical solution of the eikonal–transport equation works fine in the vicinity of the focal point, but breaks shortly beyond the focal point because of the wavefront triplication. Since the distance of applicability of the eikonal–transport equation beyond the focal point decreases with increasing frequency, see equations (17) and (19), we choose the relatively low frequency of 10 Hz. For higher frequencies, the numerical solution of the eikonal–transport equation becomes unstable within the model volume, i.e., for $x^1 < 1.000\,\mathrm{km}$.

In order to avoid problems with the bottom and top boundaries of the 2–D model volume, we extend the computational volume by 2Λ at the bottom and by 2Λ at the top, to the range from $x^3 = -2.600\,\mathrm{km}$ at the bottom to $x^3 = 1.600\,\mathrm{km}$ at the top, but display here the range from $x^3 = -1.000\,\mathrm{km}$ at the bottom to $x^3 = 0.000\,\mathrm{km}$ at the top only.

We compare the numerical solution of the eikonal–transport equation with the summation of Gaussian beams. We use the high–frequency asymptotic decomposition of the initial conditions into Gaussian beams according to Klimeš (1984). We choose the Gaussian beams with their waists situated 0.500 km along the axial ray from the initial line, and as narrow as possible at the initial line. These Gaussian beams are too narrow to be accurate in the vicinity of the caustic, but the high–frequency asymptotic decomposition of the initial conditions becomes very inaccurate for broader Gaussian beams at our low frequency of 10 Hz. The complex–valued travel time

$$\tau_{\mathrm{GB}} = \tfrac{1}{\mathrm{i}\omega} \ln(u_{\mathrm{GB}}) \tag{58}$$

corresponding to the summation u_{GB} of Gaussian beams is displayed in Figures 3 and 5.

The high–frequency asymptotic decomposition of the initial conditions into Gaussian beams is considerably inaccurate, which can clearly be observed in Figure 5, where the imaginary part of the initial travel time is not exactly equal to zero, i.e., where the left–hand side of the model volume is not exactly yellow. In our example, this inaccurate decomposition seems to represent the main inaccuracy of the Gaussian beam summation. To avoid this inaccuracy due to the decomposition of initial conditions, we use the summation of Gaussian beams along the initial line and equation (58) rather than (56) as the initial conditions for the numerical solution of the eikonal–transport equation. The initial lateral derivatives $T_1 = \tau_{,3}$ along the initial line are calculated from initial complex–valued travel time (58) by finite differences.

We apply very primitive version of coding the numerical solution of the eikonal–transport equation described in preceding Section 4, in which the system of surfaces for calculation of travel time is formed by vertical lines. The spacing between the vertical lines is decreased to 0.002 km in order to stabilize the numerical solution. We thus have 501 vertical lines between $x^1 = 0.000\,\mathrm{km}$ and $x^1 = 1.000\,\mathrm{km}$. We select 201 discrete points along each vertical line between $x^3 = -1.000\,\mathrm{km}$ and $x^3 = 0.000\,\mathrm{km}$. We use 7 iterations to solve equations (42) to (47) with $T_{abcd} = 0$. For stabilization (52), we use $q = 0.0001$.

The complex–valued travel time at frequency 10 Hz calculated by the numerical zero–order solution of the eikonal–transport equation is displayed in Figures 4 and 6.

The difference of the Gaussian beam summation from the numerical zero–order solution of the eikonal–transport equation is displayed in Figures 7 and 8. It is possible that a considerable part of the difference is caused by too narrow Gaussian beams.

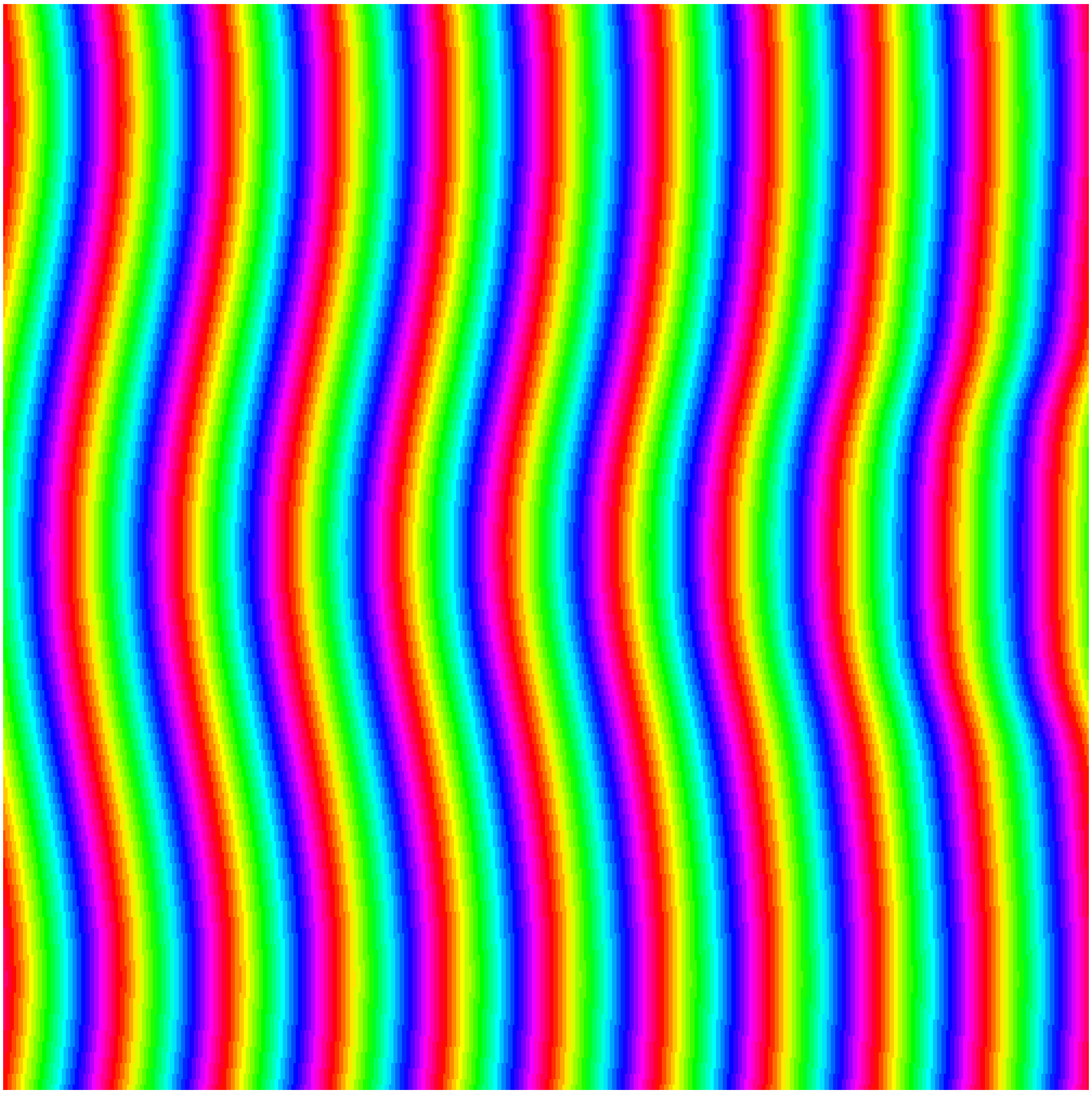

Figure 3. The real part of travel time at frequency 10 Hz calculated by the Gaussian beam summation for the approximately cosine real part of initial travel time in the real–valued homogeneous velocity model with velocity $1\,\mathrm{km\,s^{-1}}$. The values of the real part of travel time range from -0.024 s to 1.013 s. The colour circle corresponds to the time increment of 0.100 s, i.e., to 1 wavelength. The yellow colour corresponds to values 0.000 s, 0.100 s, 0.200 s, etc.

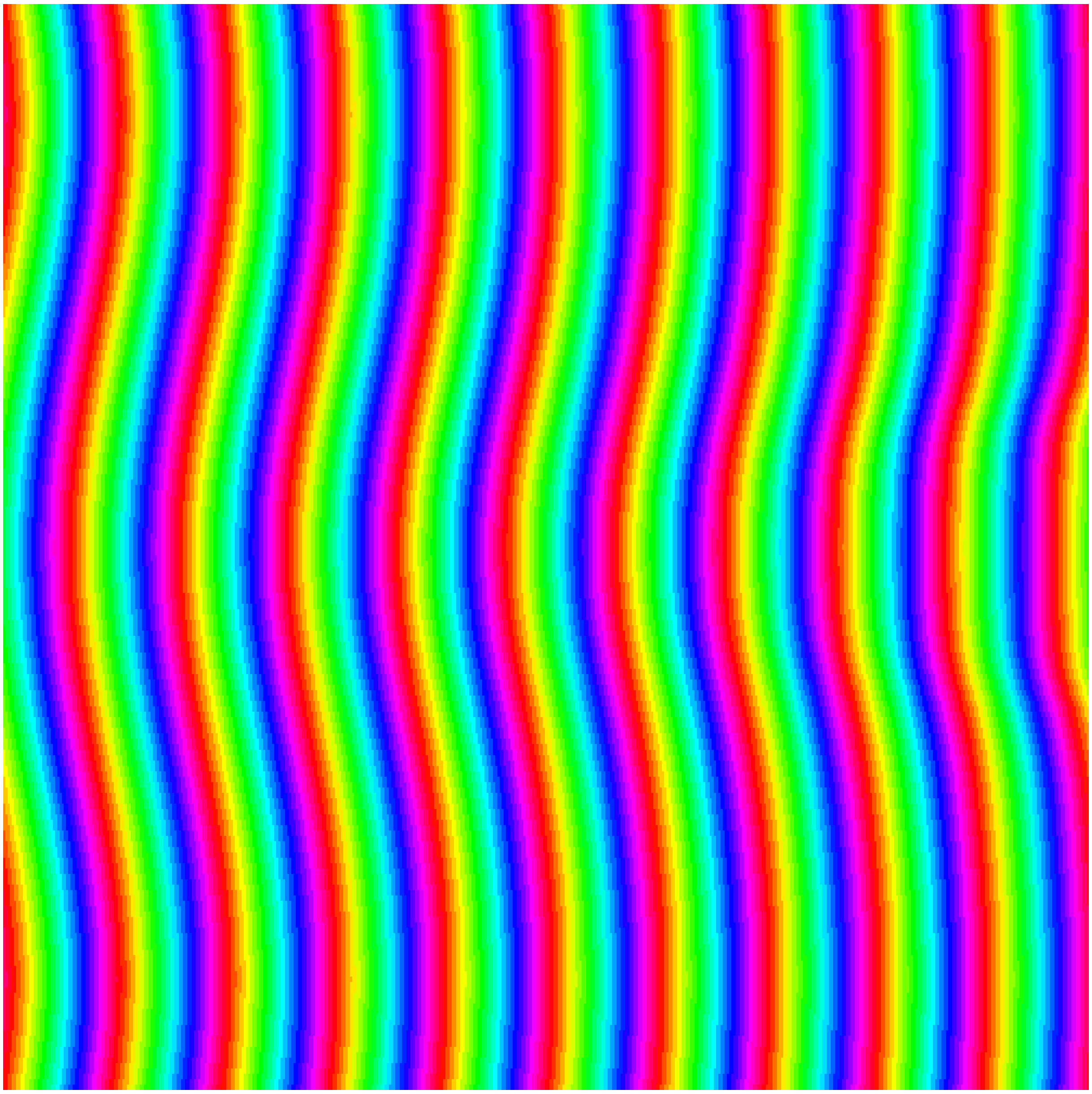

Figure 4. The real part of travel time at frequency 10 Hz calculated by the eikonal–transport equation for the approximately cosine real part of initial travel time in the real–valued homogeneous velocity model with velocity $1\,\mathrm{km\,s^{-1}}$. The values of the real part of travel time range from -0.024 s to 1.013 s. The colour circle corresponds to the time increment of 0.100 s, i.e., to 1 wavelength. The yellow colour corresponds to values 0.000 s, 0.100 s, 0.200 s, etc.

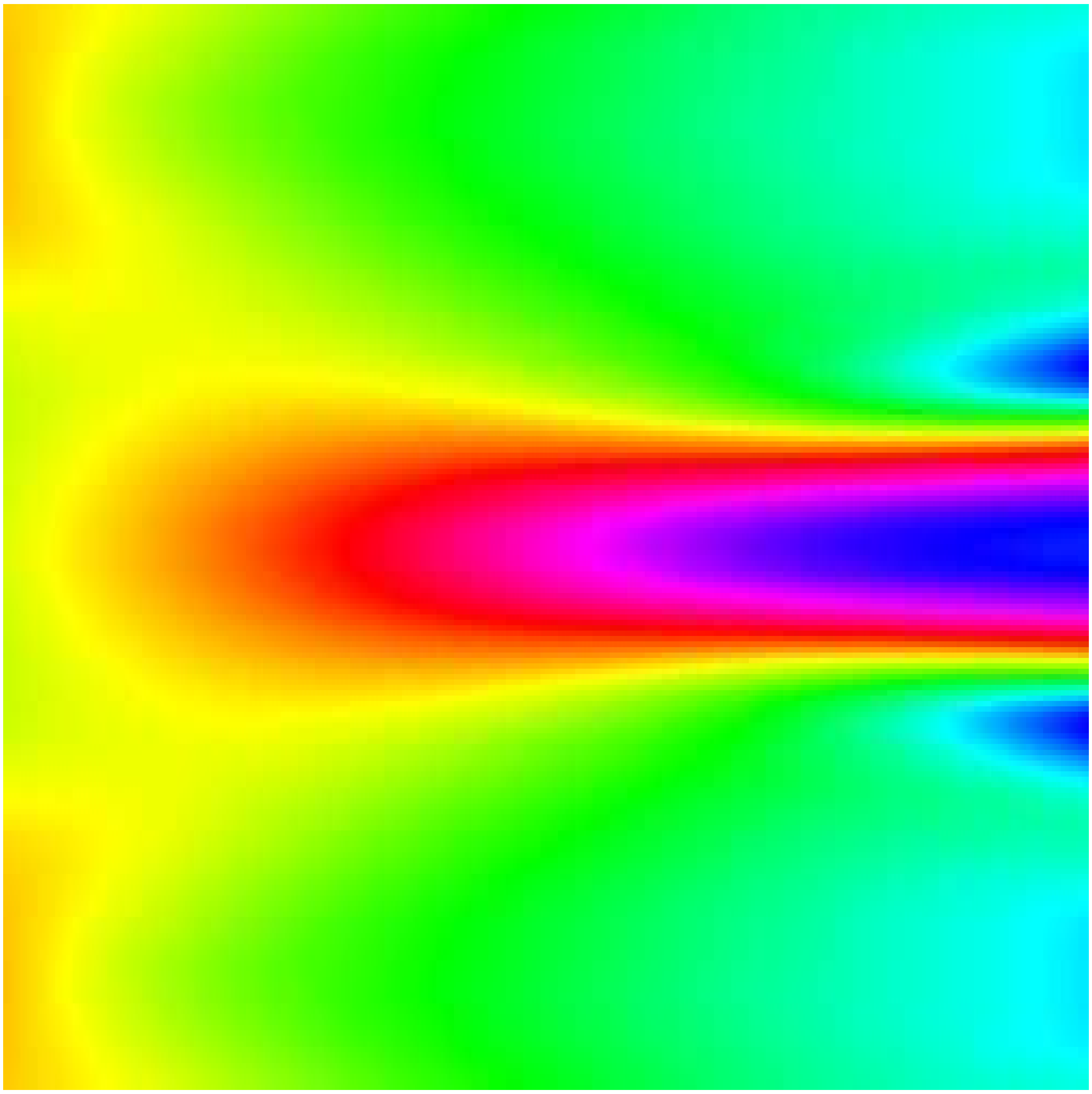

Figure 5. The imaginary part of travel time at frequency 10 Hz calculated by the Gaussian beam summation for the approximately cosine real part of initial travel time in the real–valued homogeneous velocity model with velocity $1\,\mathrm{km\,s^{-1}}$. The values of the imaginary part of travel time range from -0.010 s to 0.010 s. The colour circle corresponds to the time increment of 0.020 s. The yellow colour corresponds to value 0.000 s.

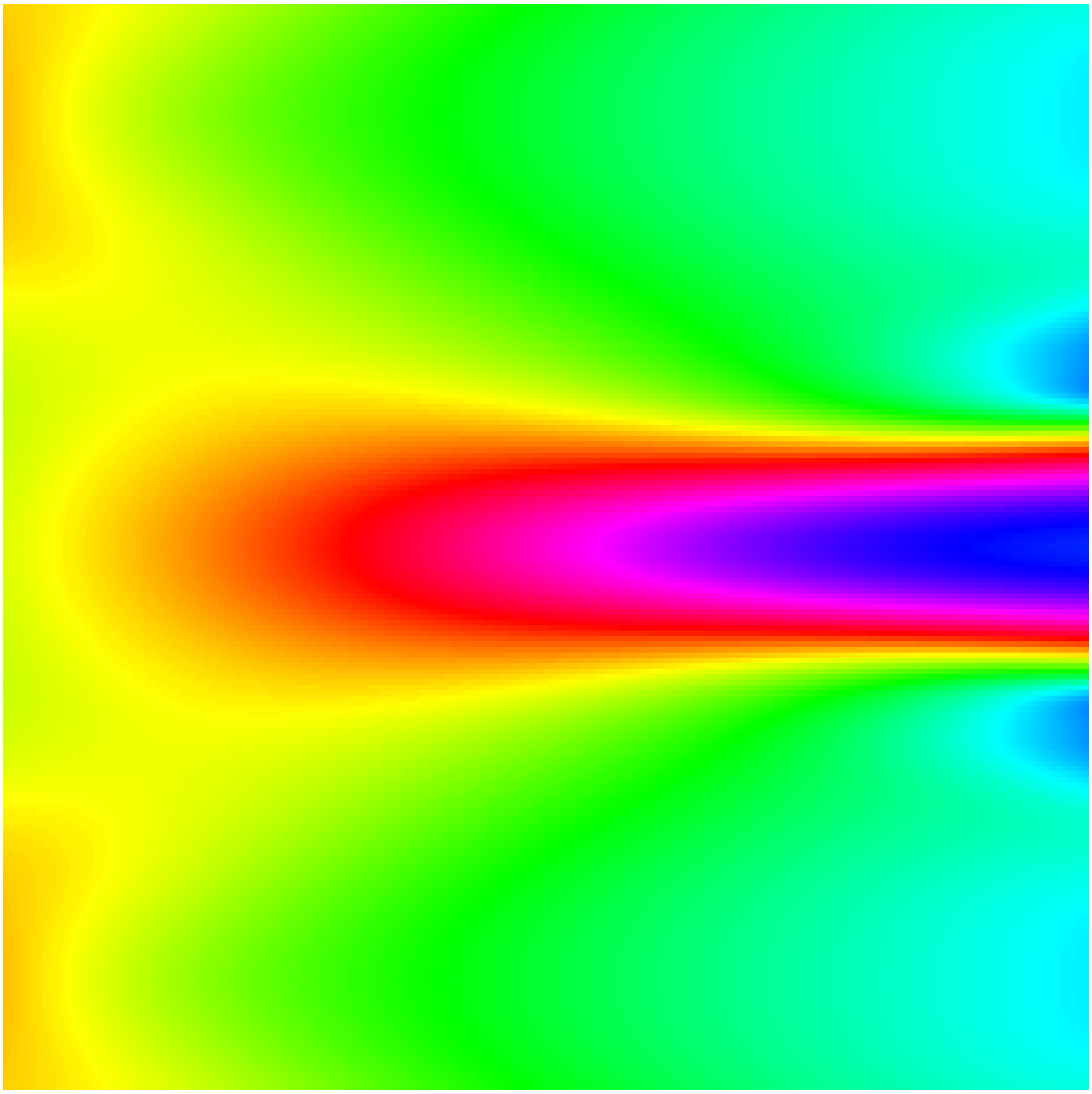

Figure 6. The imaginary part of travel time at frequency 10 Hz calculated by the eikonal–transport equation for the approximately cosine real part of initial travel time in the real–valued homogeneous velocity model with velocity $1\,\mathrm{km\,s^{-1}}$. The values of the imaginary part of travel time range from -0.010 s to 0.008 s. The colour circle corresponds to the time increment of 0.020 s. The yellow colour corresponds to value 0.000 s.

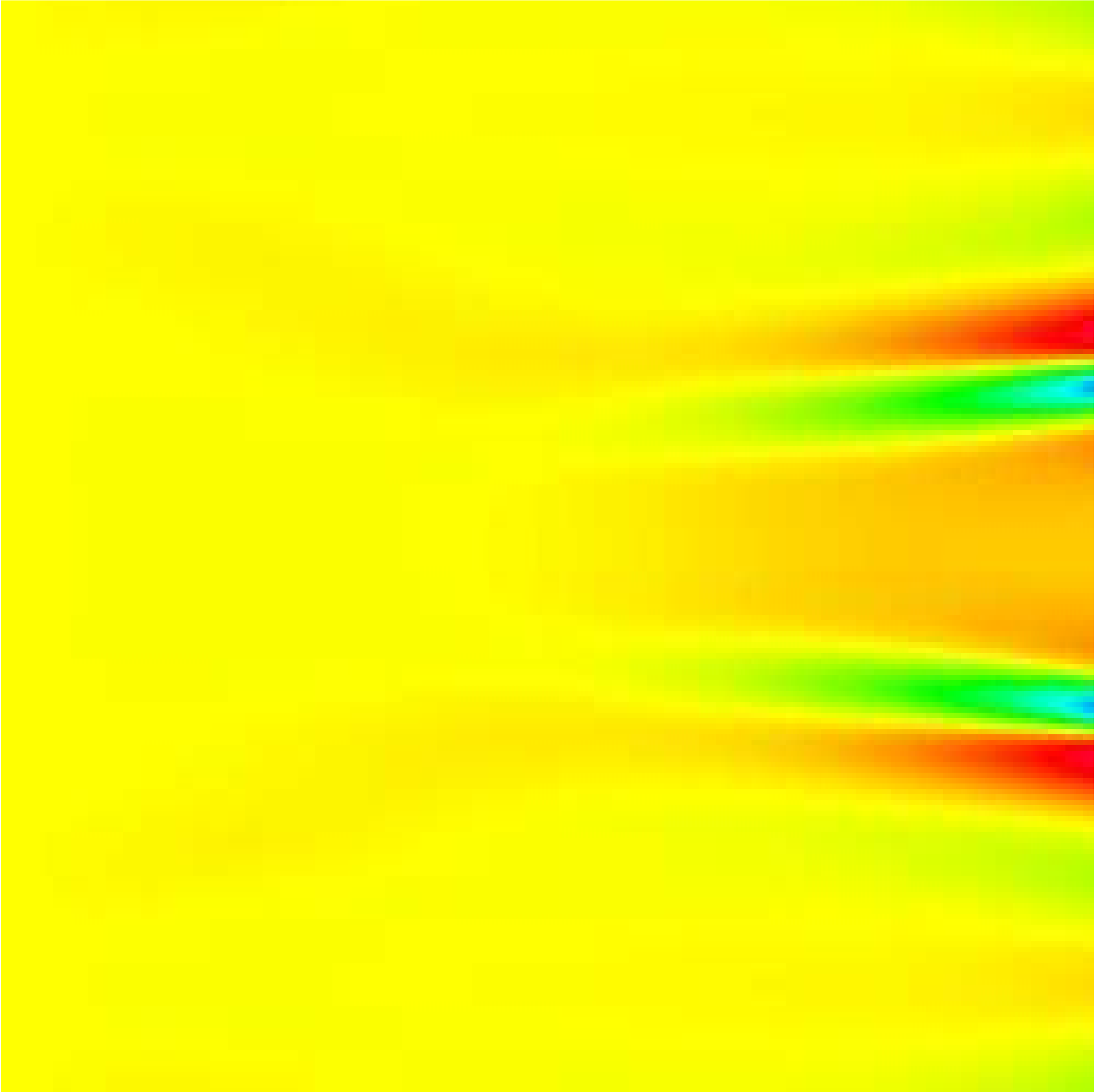

Figure 7. The difference of the real part of travel time between the Gaussian beam summation (Figure 3) and the eikonal–transport equation (Figure 4). The values of the difference range from $-0.001\,0$ s to $0.002\,0$ s. The colour circle corresponds to the time increment of 0.005 s. The yellow colour corresponds to value 0.000 s.

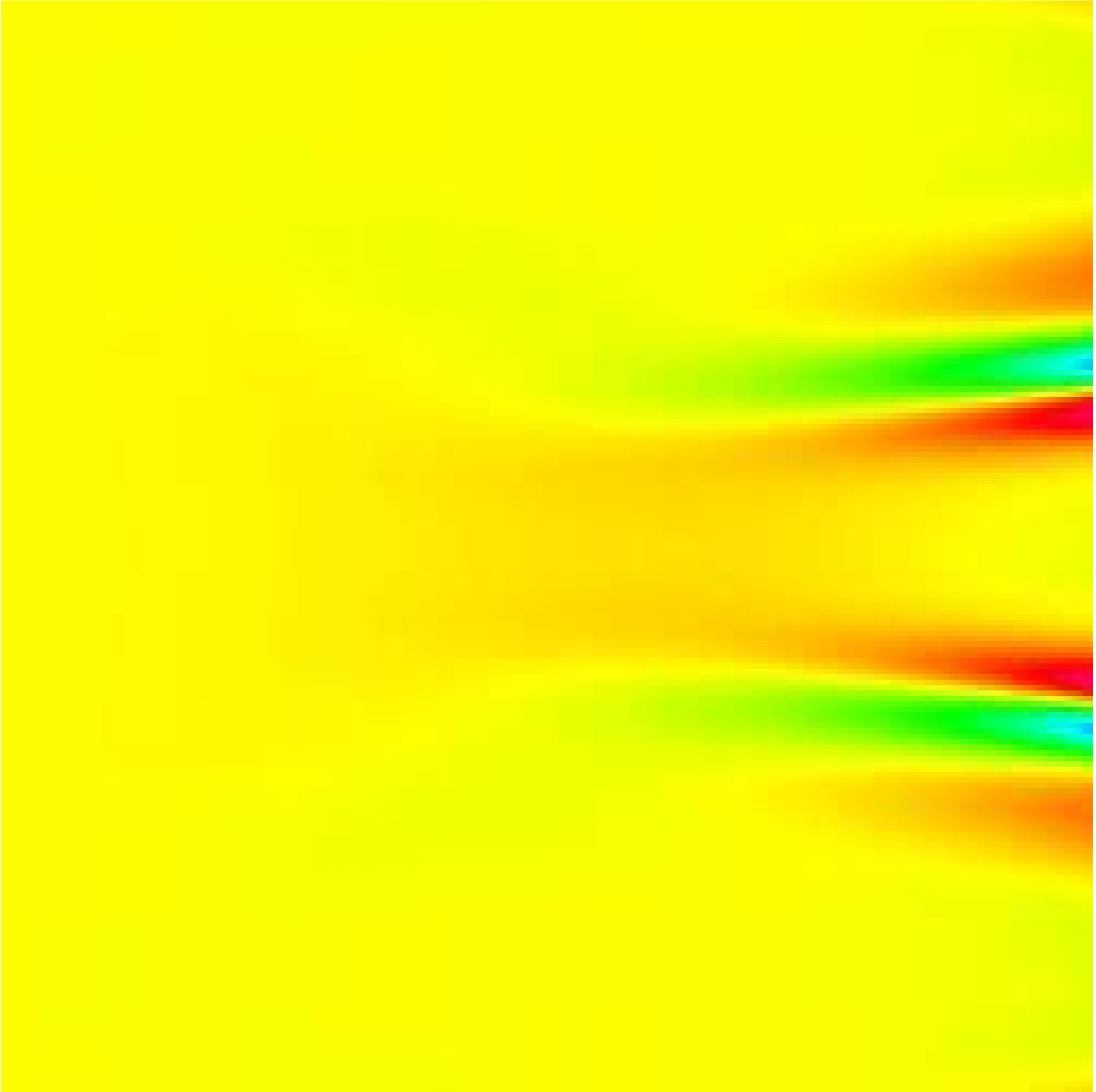

Figure 8. The difference of the imaginary part of travel time between the Gaussian beam summation (Figure 5) and the eikonal–transport equation (Figure 6). The values of the difference range from -0.0011 s to 0.0019 s. The colour circle corresponds to the time increment of 0.005 s. The yellow colour corresponds to value 0.000 s.

6. Conclusions

The complex–valued eikonal–transport equation can be applied to a wavefield with single–valued travel time and non–vanishing amplitude. Applicability of the eikonal–transport equation is thus conditioned by solving the problem of separating the solution of the eikonal–transport equation into 3 branches in a vicinity of wavefront triplication.

Acknowledgements

The research has been supported by the Grant Agency of the Czech Republic under contract 205/07/0032, by the Ministry of Education of the Czech Republic within research project MSM0021620860, and by the members of the consortium "Seismic Waves in Complex 3–D Structures" (see "http://sw3d.cz").

References

Klimeš, L. (1984): Expansion of a high–frequency time–harmonic wavefield given on an initial surface into Gaussian beams. *Geophys. J. R. astr. Soc.*, **79**, 105–118.

Klimeš, L. (1996): Grid travel–time tracing: second–order method for the first arrivals in smooth media. *Pure appl. Geophys.*, **148**, 539–563.

Klimeš, L. (2009): System of two Hamilton–Jacobi equations for complex–valued travel time. In: *Seismic Waves in Complex 3-D Structures, Report 19*, pp. 157–171, Dep. Geophys., Charles Univ., Prague.

Podvin, P. & Lecomte, I. (1991): Finite difference computation of traveltimes in very contrasted velocity models: a massively parallel approach and its associated tools. *Geophys. J. int.*, **105**, 271–284.

Vinje, V., Iversen, E. & Gjøystdal, H. (1993): Traveltime and amplitude estimation using wavefront construction. *Geophysics*, **58**, 1157–1166.

Vinje, V., Iversen, E., Åstebøl, K. & Gjøystdal, H. (1996): Estimation of multivalued arrivals in 3D models using wavefront construction — Part I. *Geophys. Prospecting*, **44**, 819–842.